

Homogenous nodal superconductivity coexisting with inhomogeneous charge order in strongly underdoped $\text{Bi}_2\text{Sr}_2\text{CaCu}_2\text{O}_{8+\delta}$

K. McElroy

*Physics Department, University of California, Berkeley, CA 94720 USA
LASSP, Department of Physics, Cornell University, Ithaca, NY 14850 USA*

D.-H. Lee

*Physics Department, University of California, Berkeley, CA 94720 USA
Material Sciences Division, Lawrence Berkeley National Lab., Berkeley, CA 94720 USA*

J. E. Hoffman

Department of Applied Physics, Stanford University, Stanford, CA 94305, USA

K. M Lang

Department of Physics, Colorado College, CO 80305, USA

E. W. Hudson

Department of Physics, MIT, Cambridge MA 02139, USA

H. Eisaki

AIST, 1-1-1 Central 2, Umezono, Tsukuba, Ibaraki, 305-8568 Japan

S. Uchida

Department of Physics, University of Tokyo, Tokyo, 113-8656 Japan

J. Lee and J.C. Davis

LASSP, Department of Physics, Cornell University, Ithaca, NY 14850 USA

(Dated: October 5, 2018)

We use novel STM techniques in concert to study the doping dependence of electronic structure in $\text{Bi}_2\text{Sr}_2\text{CaCu}_2\text{O}_{8+\delta}$. At all dopings, the low energy states are relatively homogenous except for dispersive density-of-states modulations whose properties are used to elucidate the momentum-space characteristics of quasi-particles. The superconductive coherence-peaks, ubiquitous in near-optimal tunneling spectra, are destroyed with strong underdoping. A new spectral type, likely characteristic of the zero temperature pseudogap regime, appears in these samples. Exclusively in regions exhibiting this new spectrum, we find quasi periodic modulations in dI/dV as well as in topography, with $\vec{Q} = (\pm 2\pi/4.5a_0, 0)$ and $(0, \pm 2\pi/4.5a_0) \pm 15\%$. This is consistent with the existence of a local charge density modulation at these wave vectors. Surprisingly, this state coexists harmoniously with the low energy nodal quasi-particles. We discuss the relevance of these findings to the cuprate phase diagram and to the relationship between the pseudogap and superconductivity.

High temperature superconductivity emerges in the cuprates when localized electrons in the CuO_2 plane become itinerant due to hole-doping.¹ A schematic diagram of the dependence of their electronic/magnetic characteristics on temperature (T), and doped-hole density (p), is shown in

Fig. 1 (adapted from Ref. 2). This is referred to colloquially as the cuprate 'phase-diagram' although true electronic phases (antiferromagnetic insulator (AFI), superconductor (SC) and metal (M)) have been identified in only three of its regions. Among the other poorly understood and sometimes overlapping regions are those characterized by a 'pseudogap' (PG),^{1,2,3} as a disordered magnetic 'spin glass' (SG) with incommensurate spin fluctuations,^{4,5} and as a non-Fermi liquid (NFL).^{3,6} Although no widely accepted theory exists for these phenomena, research into the underdoped cuprates

($p < 0.16$) is primarily motivated by two (apparently) distinct points of view. In the first, another electronic phase (ordered state) competes with the superconductivity. This state is thought to drive the superconducting critical temperature T_c to zero as it strengthens with reduced doping, and to disappear near maximum T_c at a hidden quantum critical point (X in Fig. 1). Within this picture, the pseudogap is primarily a property of an unknown electronic ordered state. The second picture is one in which, because of low superfluid density at low doping in two dimensions, superconductivity is destroyed by order-parameter phase and/or amplitude fluctuations and, as superfluid density rises with increased hole-doping, the T_c rises. From this perspective, the pseudogap characterizes a region above T_c exhibiting gaps in the spin and charge spectrum due to the existence of singlet pairs, even though the material is not

a superconductor. Here we report on doping-dependent STM studies of $\text{Bi}_2\text{Sr}_2\text{CaCu}_2\text{O}_{8+\delta}$ (Bi-2212), designed to explore these two models.

A serious complication for experimental exploration of these ideas is the fact that real-space (\vec{r} -space) probes generally detect nanoscale spatial heterogeneity in the electronic/magnetic structure of underdoped cuprates. For example, when $0.03 < p < 0.14$, muon spin rotation (μSR) studies indicate the existence of a disordered magnetic 'spin glass' in $\text{La}_{2-x}\text{Sr}_x\text{CuO}_4$ (La-214) and oxygen doped $\text{LaCuO}_{4+\delta}$,⁷ and in $\text{Bi}_2\text{Sr}_2\text{CaCu}_2\text{O}_{8+\delta}$ (Bi-2212).⁸ Scanning tunneling microscopy (STM) based local-density-of-states (LDOS) imaging reveals nanoscale electronic structure variations in (Bi-2212)^{9,10,11,12,13} and in $\text{Na}_x\text{Ca}_{2-x}\text{CuO}_2\text{Cl}_2$.¹⁴ Nuclear magnetic resonance (NMR) points to strong nanoscale carrier density disorder with variations in local p of at least 25% of mean carrier density in both underdoped La-214^{15,16} and underdoped Bi-2212.¹⁷ For a wide variety of underdoped cuprates, scaling analyses of penetration depth measurements reveal finite size effects consistent with nanoscale heterogeneity in the superfluid density.¹⁸ These results provide abundant independent evidence that spin and charge degrees of freedom are heterogeneous at the nanoscale in many underdoped cuprates. It has not yet been possible to determine if this heterogeneity is a sample-specific and extrinsic effect due to crystal, dopant, or chemical disorder, or is an intrinsic effect of the cuprate electronic structure. Nor have its implications for the phase diagram been considered widely.

A complementary description of electronic structure to that in \vec{r} -space is in momentum space (\vec{k} -space), accessible for cuprates via angle resolved photoemission (ARPES), and optical techniques. ARPES reveals that, at optimal p in the superconducting phase, the Fermi-surface (FS) of hole-doped cuprates is gapped by an anisotropic energy gap $\Delta(\vec{k})$ with four nodes, and, below T_c , quasiparticles exist everywhere along the normal-state Fermi surface.^{19,20,21} At a fixed low temperature, those quasi-particle states with $\vec{k} = (\pm\pi/a_0, 0)$ and $(0, \pm\pi/a_0)$ near the 1st Brillouin zone-face, degrade rapidly in coherence with reduced doping until they have become incoherent at $p < 0.10$.^{19,20,22,23} This is a mysterious phenomenon, since it is closely correlated with superfluid density²⁴ but, within conventional superconductivity theories, should not be related to it. By contrast, states on the 'Fermi-arc' (FA)²⁵ nearby the nodes retain their coherence down to the lowest dopings studied.^{19,26,27} Transient grating optical spectroscopy studies of non-equilibrium quasi-particles in underdoped $\text{YBa}_2\text{Cu}_3\text{O}_{6.5}$ ²⁸ also find lifetimes for antinodal excitations that are orders of magnitude shorter than those of the nodal quasi-particles. Thus, the electronic structure of underdoped cuprates also appears to be heterogeneous in \vec{k} -space, in the sense that states proximate to the gap-nodes (nodal) have quite different characteristics and evolution with doping, than those near the zone-face (antinodal). No generally accepted explana-

tion exists for either these \vec{k} -space phenomena or their relationship to the phase diagram.

An electronic structure like this, which is heterogeneous in both \vec{r} -space and \vec{k} -space, presents special challenges to conventional experimental techniques. Nevertheless for the cuprates, it is critical to understand the relationship between these two electronic structure representations and how it evolves with doping. Here, by using several innovative STM techniques in concert, we have carried out the first comprehensive study of the doping dependence of Bi-2212 superconducting electronic structure in \vec{r} -space and determined its relationship to the electronic structure in \vec{k} -space. Our first technique is local density of states (*LDOS*) mapping which consists of measurement of the tip-sample differential tunneling conductance $g(\vec{r}, V) \equiv \frac{dI}{dV}|_{\vec{r}, V}$ at each spatial location and at each sample bias voltage V . Since $LDOS(\vec{r}, E = eV) \propto g(\vec{r}, E = eV)$, an energy-resolved \vec{r} -space image of the electronic structure is attained. Second, from $g(\vec{r}, E)$ a dataset, the magnitude of the energy-gap in the density of states $\Delta(\vec{r})$ can be determined in a process called a gapmap. Here $\Delta(\vec{r}) \equiv \frac{\Delta(\vec{r})_+ - \Delta(\vec{r})_-}{2}$ and is the energy of the first maximum in $LDOS$ above(below) the Fermi level (neglecting impurity states).¹² A final technique, recently introduced to cuprate studies,²⁹ is Fourier transform scanning tunneling spectroscopy (FT-STs). Here, the \vec{q} -vectors of spatial modulations in $g(\vec{r}, E)$ are determined from the locations of peaks in $g(\vec{q}, E)$, the Fourier transform magnitude of $g(\vec{r}, E)$. This technique has proven valuable by virtue of its exceptional capability^{30,31,32} to relate the nanoscale \vec{r} -space electronic structure to that in \vec{k} -space.

To clarify these techniques, we show examples of each measurement type in Fig.2. All are derived from a single $g(\vec{r}, E)$ data set measured with 1.8 Å resolution in 256^2 pixels on a 50 nm -square field of view (FOV). Figure 2A is the gapmap $\Delta(\vec{r})$ from this $g(\vec{r}, E)$ using a color scale that spans $20\text{meV} < \Delta(\vec{r}) < 70\text{meV}$. The superposed inset shows the resolution of a topographic image taken precisely where this $g(\vec{r}, E)$ was measured. An example of unprocessed $g(\vec{r}, E)$ typical of strongly underdoped samples, is shown in Fig.2B. These spectra were measured along the red line in Fig 2A. From these data, one can see dramatic changes during which the coherence peaks in the spectrum disappear and are replaced by to a distinctly different type of spectrum. Such evolutions are ubiquitous in strongly underdoped Bi-2212 samples. Fig.2C is the measured $g(\vec{r}, E = -12\text{meV})$ in the FOV of 2A. It exhibits a complex pattern of very weak *LDOS* modulations which are relatively homogeneous in the sense that RMS-deviations from spatially averaged value of $g(\vec{r}, E)$ are only 10%. Fig.2D is the $g(\vec{q}, E = -12\text{meV})$ calculated from Fig.2C and it reveals that the *LDOS*-modulations in Fig.2C were made up of only a small set of well-defined \vec{q} -vectors.^{30,31}

We apply these techniques in concert to study the doping-dependence of electronic structure in a series of Bi-2212 samples. They are all single crystals grown by

the floating zone method. Doping is controlled by oxygen depletion so that no other elemental impurities are introduced. Each is cleaved in cryogenic ultra-high vacuum before immediate insertion into the STM head. If its BiO surface is flat and free of nanoscale debris, each sample is usually studied for several months, typically in a 50nm square field of view (FOV). More than 10^6 spectra were acquired for the studies reported here.

In Fig.3 we show 50nm-square gapmaps measured on samples with five different dopings. Identical color scales representing $20 \text{ meV} < \Delta(\vec{r}) < 70 \text{ meV}$ are used for all images. The local hole concentration is impossible to determine directly, but we estimate that the bulk dopings were approximately **3A**(0.19 ± 0.01), **3B**(0.18 ± 0.01), **3C**(0.15 ± 0.01), **3D**(0.13 ± 0.01), **3E**(0.11 ± 0.01). Near optimal doping (Fig 3**A,B**) the gapmaps are heterogeneous but nonetheless the vast majority of tunneling spectra are manifestly those of a superconductor (see below). However, at the lowest dopings and for gap values exceeding approximately 65 meV, there are very many spectra where Δ actually becomes ill defined because coherence peaks do not exist at the gap edge (see for example Fig.3**F**, spectrum 6). We represent these spectra by black in the gapmap, since they are almost identical to each other and appear to be the limiting class of spectra at our lowest dopings.

The spatially averaged value of $\Delta(\vec{r})$ for each crystal, $\bar{\Delta}$, and its full width at half maximum, σ , are: **3A**($\bar{\Delta} = 33 \pm 1 \text{ meV}$, $\sigma=7 \text{ meV}$), **3B**($\bar{\Delta} = 36 \pm 1 \text{ meV}$, $\sigma=8 \text{ meV}$), **3C**($\bar{\Delta} = 43 \pm 1 \text{ meV}$, $\sigma=9 \text{ meV}$), **3D**($48 \pm 1 \text{ meV}$, $\sigma=10 \text{ meV}$), and **3E**($\bar{\Delta} > 62 \text{ meV}$ but with σ ill defined). As doping is reduced, $\bar{\Delta}$ grows steadily consistent with other spectroscopic techniques, such as ARPES and break-junction tunneling,^{19,20,33} which average over the heterogeneous nanoscale phenomena. This observation is very important because it demonstrates that our Bi-2212 surfaces evolve with doping in an electronically equivalent fashion to those studied by the other techniques, and that we are probing the low temperature state of the underdoped pseudogap regime.

In Fig.3**F** we show a series of the 'gap-averaged' spectra. Each is the average spectrum of all regions exhibiting a given local gap value (from the single 50nm FOV of Fig.2**C**). They are color-coded so that each gap-averaged spectrum can be associated with regions of the same colour in all gapmaps (Fig.'s 3**A-E**). The spectra are labeled from 1-6, with numbers 1 through 4 providing clear examples of what we refer to as coherence peaks at the gap edge (indicated by the arrows). These gap-averaged spectra are consistent with data reported previously by from gapmap studies by Matsuda *et al.*¹³ Here, from our doping dependence study, we can report that this set of gap-averaged spectra is almost identical for all dopings. The dramatic changes with doping seen in $\Delta(\vec{r})$ (Fig.3) occur because the probability of observing a given type of spectrum in Fig.3**F** evolves rapidly with doping. For example, the gap-averaged spectrum labeled as 1 in Fig.3**F** has a 30% probability of occurring in gapmap **3A**, 25%

in **3B**, 5% in **3C**, less than 1% in **3D**, and 0% in **3E**. The spectrum labeled 6 has a 0% probability of occurring in **3A**, 0.1% in **3B**, 1% in **3C**, 8% in **3D** and $> 55\%$ probability in **3E**. The evolution of these gapmaps (Fig.3) with falling doping, from domination by heterogeneous but predominantly superconducting spectral characteristics (Fig.3**A,B**) to domination by spectra of a very different type (Fig.3**E**) is striking.

Despite the intense changes with doping in the gapmaps (whose information content is, by definition, derived from the coherence peaks at $E = \Delta(\vec{r})$), the *LDOS* at energies below about $0.5\bar{\Delta}$ remains relatively homogeneous for all dopings studied. Figure 3**F** reveals this low-energy *LDOS* homogeneity because, independent of gap value, the $g(E)$ below $\approx 25 \text{ meV}$ are almost the same everywhere and for all spectra. These low energy *LDOS* do, however, exhibit numerous weak, incommensurate, energy-dispersive, spatial *LDOS*-modulations with long correlation lengths (for example Fig.2**C**). We focus on the doping dependence of these low energy $g(\vec{r}, E)$ data by applying the FT-STs technique. Figure

4**A-C** shows measured $g(\vec{q}, E)$ for the three $g(\vec{r}, E)$ datasets used to generate Fig.3**A**, **3D**, and **3E**. Each sub-panel is the measured $g(\vec{q}, E)$ at the labeled energy, with the reciprocal space locations of the Bi (or Cu) atoms $\vec{q} = (\pm 2\pi/a_0, 0)$ and $(0, \pm 2\pi/a_0)$, appearing as the four dark spots at the corners of a square. It is obvious that multiple sets of dispersive *LDOS*-modulations exist at all three dopings, but each exhibits different trajectories as a function of E for different p .

Analysis of these low energy *LDOS* modulations requires a model for their relationship to states in \vec{k} -space. We apply the 'octet model' of quasiparticle interference^{30,31} which is predicated on a Bi-2212 superconducting band-structure exhibiting four sets of 'banana'-shaped contours of constant quasiparticle-energy surrounding the gap nodes.¹⁹ Because of the quasiparticle density of states at E is

$$n(E) \propto \oint_{E(\vec{k})=E} \frac{1}{\nabla_{\vec{k}} E(\vec{k})} d\vec{k} \quad (1)$$

while each 'banana' exhibits its largest $|\nabla_{\vec{k}} E(\vec{k})|^{-1}$ near its two ends, the primary contributions to come from the octet of momentum-space regions at the ends of each 'banana' \vec{k}_j ; $j=1,2,\dots,8$ (Fig.5**A**). Mixing of quasiparticle states in the octet by disorder scattering produces quasiparticle interference patterns which are manifest as spatial *LDOS*-modulations. The intensity of such scattering induced modulations is primarily governed by joint density of states (among other factors). The wavevectors of the most intense *LDOS*-modulations are then determined by all possible pairs of points in the octet \vec{k}_j . Sixteen distinct $+\vec{q}$ and $-\vec{q}$ pairs should be detectable at each non-zero energy by FT-STs. From them, the energy dependence of the octet locations $\vec{k}_j(E)$ can be determined and associated with a 'locus of scattering' $\vec{k}_s(E)$. Comprehensive internally-consistent agreement between Bi-

2212 STM data and this model is achieved near optimal doping.³¹ Until this work, nothing was known about its utility for strongly underdoped cuprates.

Theoretical analyses beyond the simple octet model^{34,35,36,37,38,39,40,41,42,43} capture many elements of our previously reported $g(\vec{q}, E)$ data, but no resolution of the exact source, strength, or type of scattering has yet been achieved. Nevertheless, the existence of numerous sets of long-correlation length, dispersive, $LDOS$ modulations, all of which are self-consistent with a single $\Delta(\vec{k})$ for both filled and empty states, is indicative of good Bogoliubov-like quasi-particles. Since the $LDOS$ -modulations can be associated consistently with a 'locus of scattering' $\vec{k}_s(E)$ via the octet model, we analyze our observations within this model using the \vec{q} -vector designations shown in Fig.5A.

Figure 5B shows the measured length of \vec{q}_1 , \vec{q}_5 and \vec{q}_7 as a function of energy for the three datasets in Fig.4. Figure 5C shows the locus of scattering calculated for these three using:

$$\begin{aligned} \vec{q}_1 &= (2k_x, 0); \vec{q}_5 = (0, 2k_y); \vec{q}_7 = (k_x - k_y, k_y - k_x) \quad (2) \\ \vec{k}_s &= (\pm k_x(E), \pm k_y(E)); \vec{k}_s = (\pm k_y(E), \pm k_x(E)) \quad (3) \end{aligned}$$

The $\vec{k}_s(E)$ determined by this technique differs only slightly between dopings. even though the actual $g(\vec{r}, E)$ for different dopings are quite different at any given energy. These three $\vec{k}_s(E)$ are each the same for filled and empty sates and each consistent with the same $\Delta(\vec{k})$ at that doping. Thus Bogoliubov-like quasi-particles appear to exist at these momentum space locations at all dopings. This is consistent with the small motion of the FS in this doping range detected by ARPES.

These observations certainly do not exhaust the changes observed in $g(\vec{r}, E)$ with falling doping. A very strong effect is the evolution, with doping, of the \vec{q} -space location of strongest $LDOS$ -modulation at any energy. This modulation is always associated with \vec{q}_1 and vits location evolves from $\vec{q}_1 = \frac{2\pi}{6a_0}$ at $p= 0.19 \pm 0.01$, to $\vec{q}_1 = \frac{2\pi}{5.1a_0}$ at $p= 0.14 \pm 0.01$, to $\vec{q}_1 = \frac{2\pi}{4.7a_0}$ at $p= 0.10 \pm 0.01$. Another effect is a decrease in relative intensity of dispersive $LDOS$ -modulations \vec{q}_2 , \vec{q}_3 , \vec{q}_6 , \vec{q}_7 relative to those of \vec{q}_1 , \vec{q}_5 , with falling with p . These effects will be reported in detail elsewhere.

The doping dependence of states with $\vec{k} = (\pm\pi/a_0, 0)$ and $(0, \pm\pi/a_0)$ in the 'flat band' region near the zone-face¹⁹ (green shaded areas in Fig.5A) is extremely different. These states can also be identified by FT-STS analysis of $g(\vec{r}, E)$ data. By definition, the coherence peaks in $g(\vec{r}, E)$ occur at $E = \Delta(\vec{r})$. In all samples, they exhibit intense particle-hole symmetric $LDOS$ -modulations, with wavevectors $\vec{G} = (\pm 2\pi/a_0, 0)$ and $(0, \pm 2\pi/a_0)$.³¹ These coherence peak $LDOS$ -modulations at $E = \Delta$ possibly occur due to Umplapp scattering between $\vec{k} = (\pm\pi/a_0, 0)$ and $(0, \pm\pi/a_0)$.³¹ Therefore, the coherence peaks in tunneling are identified empirically with the zone-face states

at $\vec{k} = (\pm\pi/a_0, 0)$ and $(0, \pm\pi/a_0)$. This identification is also consistent with theory. The coherence peaked tunneling spectra (e.g. Fig.2F: spectra 1-4) are theoretically viewed as due to superconducting pairing on the whole FS because such spectra are consistent with a $\Delta_{x^2-y^2}$ everywhere on the ARPES-determined FS near optimal doping.³ We therefore consider any spatial regions that show clear coherence peaks with $\vec{q} = \vec{G}$ $LDOS$ -modulations, to be occupied by a canonical d-wave superconductor (dSC).

Near optimal doping, more than 98% of any FOV exhibits this type of coherence peaked dSC spectrum. As the range of local values of $\Delta(\vec{r})$ increases with decreasing doping, the intensity of the $\vec{q} = \vec{G}$ coherence peak $LDOS$ -modulations becomes steadily weaker until, wherever $\Delta(\vec{r}) > 65$ meV, they disappear altogether. This process can be seen clearly in the gap-averaged spectra of Fig.3F where the average height of the coherence peaks declines steadily with increasing Δ . It is found equally true for all dopings. Wherever the coherence peaks and their $\vec{q} = \vec{G}$ $LDOS$ -modulations are absent, a well-defined new type of spectrum is always observed. Figure 6A shows a high resolution gapmap from a strongly underdoped sample. Examples of this new type of spectrum, along with those of coherence peaked dSC spectra, are shown in Fig.6B. The coherence peaked spectra (red) are manifestly distinct from the novel spectra (black) which have a V-shaped gap reaching up to -300 meV and +75 meV. For reasons to be discussed below, we refer to the new spectrum as the zero temperature pseudogap (ZTPG) spectrum.

The replacement of coherence peaked dSC spectra by ZTPG spectra first begins to have strong impact on averaged properties of $g(\vec{r}, E)$ and $g(\vec{q}, E)$ below about $p=0.14$ where the fractional area covered by ZTPG spectra first exceeds 10% of the FOV. In terms of the spectral shape no further evolution in the form of the ZTPG spectrum is detected at lower dopings. Instead, a steadily increasing fractional coverage of the surface by these ZTPG spectra is observed. Our previous studies^{10,12} were carried out at dopings $p > 0.14$ and, when ZTPG spectra have been detected at such higher dopings,^{10,11} it is in a tiny fraction of the FOV. Very significantly, spectra similar to the ZTPG spectrum are detected inside cores of Bi-2212 quantized vortices where superconductivity is destroyed.^{44,45} Furthermore, a very similar spectrum is observed in another very underdoped cuprate $\text{Na}_x\text{Ca}_{2-x}\text{CuO}_2\text{Cl}_2$,^{14,46} even in the non-superconducting phase. It therefore seems reasonable that the characteristic zero-temperature spectrum in the pseudogap phase is of this type. This is why we tentatively assign this spectrum the ZTPG designation.

As discussed above, the $g(\vec{r}, E)$ for $E < \bar{\Delta}/2$ in even the most underdoped samples (Fig.3E, Fig.4C) exhibit relatively homogenous electronic structure with good quasi-particles dispersing on the Fermi-arc. However, for $E > \bar{\Delta}/2$ in these same samples, our previous analyses techniques fail, probably because very different phenom-

ena are occurring in different nanoscale regions of each FOV. To explore the implications of the ZTPG spectrum for strongly underdoped samples, new analysis techniques are therefore required. Here we introduce a masking process which has proven highly effective. From a given strongly underdoped data set, the $g(\vec{r}, E)$ in all regions where $E\Delta > 65$ meV are excised and used to form a new masked data set $g(\vec{r}, E)|_{\Delta > 65}$. The remainder forms a second new dataset $g(\vec{r}, E)|_{\Delta < 65}$. The $E\Delta > 65$ meV cutoff was chosen because, on the average, it represents where the coherence peaks with associated $\vec{q} = \vec{G}$ modulations have all disappeared and are replaced by the ZTPG spectra. An example of this type of mask for the gapmap in Fig.6A is show in Fig.5C. It is important to note a serious drawback of the masking process. The \vec{q} resolution is of masked data is considerably worse in than those shown in Fig.5B because the largest contiguous nano region in the mask is about 20% of the full FOV. As a result, the precise modulation period and dispersions of any effects detected by masking cannot can be determined with nearly the same degree of accuracy as the low-energy quasi-particle interference signal (Fig.5 and Ref. 28).

FT-STs analysis of such $(g(\vec{r}, E)|_{\Delta < 65}, g(\vec{r}, E)|_{\Delta > 65})$ pairs shows that they exhibit dramatically different phenomena. In the $g(\vec{r}, E)|_{\Delta < 65}$, the dispersive trajectory of \vec{q}_1 is seen up to $E \approx 36$ meV and no further *LDOS*-modulations can be detected at any higher energy (red symbols in Fig.6D). In the $g(\vec{r}, E)|_{\Delta > 65}$ data, the identical dispersive \vec{q}_1 signal is seen below E 36 meV. However, a new *LDOS*-modulation appears in the $g(\vec{r}, E)|_{\Delta > 65}$ between $E > 65$ meV and our maximum energy $E=150$ meV (black symbols in Fig.6D). We designate its wavevector \vec{q}^* .

To explore the real-space structure of this new high-energy *LDOS*-modulation, we define a map $\Gamma_{65}^{150}(\vec{r}) = \Sigma_{E=65}^{150} g(\vec{r}, E)|_{\delta > 65}$ which sums over this energy range. This map is shown in Fig.7A and, although it has quite a disordered mask, careful examination reveals checkerboard modulations within each nano region. Importantly, Fourier transform analysis of this $\Gamma_{65}^{150}(\vec{r})$ shown in Fig. 7B reveals a well-defined wavevector set $\vec{q}^* = (\pm 2\pi/4.5a_0, 0)$ and $(0, \pm 2\pi/4.5a_0) \pm 15\%$ for these new high-energy modulations as indicated by the arrow on black data points in inset to Fig. 7B. The identical analysis the complementary map $\Sigma_{65}^{150} g(\vec{r}, E)|_{\delta < 65}$ is featureless near \vec{q}^* (red data in inset of Fig. 7B). Thus, an *LDOS*-modulation with very low (or zero) dispersion, exists above ± 65 meV exclusively in regions characterized by ZTPG spectra of strongly underdoped Bi-2212 samples.

Constant-current topography represents, albeit logarithmically, the contour of constant integrated density of states up to the sample-bias energy. It does not suffer from the systematic problems due to effects of the constant-current setup condition renormalization¹⁰ which plague $g(\vec{r}, E)$. It is therefore a more conclusive technique for detection of net charge density modulations

by STM. To search for topographic modulations, we apply the identical mask (Fig.7C) to the topographic image which was acquired simultaneously with the gapmap in 6A. The magnitude of the Fourier transform along the $\vec{q}|| (2\pi, 0)$ for the masked topographic image shows that, in the ZTPG regions, the topography is modulated with $\vec{q}_{topo} = (\pm 2\pi/5a_0, 0)$ and $(0, \pm 2\pi/5a_0) \pm 25\%$ (indicated by the arrows in Fig.7D). Fourier transforms of the complementary part of the topography (from $\Delta < 65$ meV regions not exhibiting ZBTG spectra) shows no such modulations at any wavelengths near this \vec{q}_{topo} (red in Fig.7C). No topographic modulations near \vec{q}_{topo} are detected anywhere in samples at higher doping. An additional peak near $\vec{q}_{recon} = (2\pi/2a_0, \pm 2\pi/2a_0)$ and $(-2\pi/2a_0, -2\pi/2a_0)$ in the Fourier transform of the topograph comes from a reconstruction along the supermodulation maximum, is observed at all dopings and, since no signature is observed in *LDOS* at \vec{q}_{recon} for any energy or doping, is regarded as irrelevant.

Some important new facts about the strongly underdoped regime of Bi-2212 electronic structure emerge from these results. Our first finding is related to the Fermi-arc quasi-particle states. As shown in Fig. 5C, FT-STs indicates that quasi-particle interference occurs between Bogoliubov-like states in approximately the same region of \vec{k} -space for all dopings. These Fermi-arc quasiparticles remain spatially homogenous (except for relatively weak *LDOS*-modulations) even in the most underdoped samples. They are Bogoliubov-like in the sense that they exhibit particle-hole symmetry at each location in \vec{k} -space, and, at each doping, are all consistent with the same $\Delta(\vec{k})$. Therefore, one can reasonably postulate that Fermi-arc states are gapped by superconducting interactions at all dopings studied. If so, they, and the associated 'nodal' superconducting state,^{47,48,49,50} are amazingly robust against the heterogeneous electronic phenomena which so dominate Bi-2212 at other energies.

Our second finding is the very different fate of states in the flat-band regions near $\vec{k} \approx (\pm\pi/a_0, 0); (0, \pm\pi/a_0)$. The appearance of ZTPG spectra in strongly underdoped samples coincides exactly with destruction of antinodal superconducting coherence peaks. Exclusively in these ZTPG regions (black in the gapmap), we find the three new modulation phenomena: (1) topographic modulations with $\vec{q}_{topo} = (\pm 2\pi/5a_0, 0)$ and $(0, \pm 2\pi/5a_0) \pm 25\%$, (2) a peak in *LDOS* centered around $\vec{q}^* = (\pm 2\pi/4.5a_0, 0)$ and $(0, \pm 2\pi/4.5a_0) \pm 15\%$ for $E > 65$ meV to at least $E=150$ meV and, (3) the dispersive \vec{q}_1 quasi-particle branch exhibits its maximum modulation intensity when it passes through $\vec{q}_1 = \vec{q}_{topo} = \vec{q}^*$ (Fig 7D). This last situation has been predicted^{37,38,39,41,51} as a consequence of the Fermi surface geometry and quasi-particle dispersion in the presence of potential scattering from charge-order with fixed \vec{Q} ; in this case $\vec{Q} = \vec{q}_{topo} = \vec{q}^*$. Taken together, these observations all point to the appearance of an unusual charge ordered state with $\vec{q}^* = (\pm 2\pi/4.5a_0, 0)$ and $(0, \pm 2\pi/4.5a_0) \pm 15\%$, occurring only in the regions characterized by the ZTPG spectrum and only in strongly

underdoped Bi-2212. Note that due to the strong disorder and the limited size of the mask domain we can not distinguish between a charge density modulation caused by a condensed charge order and that caused by impurity through an enhanced charge susceptibility in a state without condensed charge order.⁵² In addition we do not imply that there is true charge long range order since from the Imry-Ma argument this is always absent in a disordered system like Bi-2212.

Charge order has been observed in other underdoped cuprates, including Nd doped La-214 with inelastic neutron scattering⁵³ and more recently by STM in $\text{Na}_x\text{Ca}_{2-x}\text{CuO}_2\text{Cl}_2$.⁴⁶ It has also been proposed, based on reported nondispersive (between 0 and 20 meV), 'line object', *LDOS* modulations with $\vec{q} = (2\pi/4a_0, 0)$ ⁵⁴, that static stripes exist in optimally doped Bi-2212 below T_c . However, none of these phenomena have been detected in several independent higher resolution studies.^{30,31,32}

Other very suggestive findings have also been made by STM in Bi-2212. Field induced sub-gap *LDOS*-modulations, with $\vec{q}_{\text{vortex}} = (\pm 2\pi/4.3a_0, 0)$ and $(0, \pm 2\pi/4.3a_0) \pm 15\%$ were discovered surrounding vortex cores (where superconductivity is destroyed) near optimal doping. This observation provided the first STM evidence for some type of incipient charge-order competing with superconductivity in cuprates.²⁹ Pioneering STM experiments to map the low energy *LDOS* above T_c when superconductivity is also destroyed, have detected sub-gap *LDOS*-modulations with $\vec{q}_{PG} = (\pm 2\pi/4.6a_0, 0)$ and $(0, \pm 2\pi/4.6a_0)$ ³² at near-optimal doping. Although neither of these low energy phenomena are fully understood, they do, along with low energy phenomena in ZTPG regions reported here, form a triad of apparently consistent observations. Destruction of superconductivity, whether by high magnetic fields, by exceeding T_c , or by strong underdoping, results in very similar effects on low energy *LDOS* modulations. It remains to be determined how the vortex core and pseudogap observations relate directly to the charge order.

The identity of the electronic phase represented by the $\vec{q}_{\text{topo}} = \vec{q}^*$ charge order is difficult to discern. In the absence of disorder, plaquette orbital-order phases such as staggered flux phase (SFP)^{55,56} and D-density-wave (DDW),⁵⁷ or intra-plaquette orbital phases,⁵⁸ are not expected to exhibit topographic or *LDOS*-modulations. However, in theory, *LDOS*-modulations can be produced by vortex and disorder scattering in the SFP and DDW phases but not near $\vec{q} = (\pm 2\pi/4a_0, 0)$ and $(0, \pm 2\pi/4a_0)$.^{42,43,59} It remains theoretically unexplored whether disordered orbital phases could result in the complete set of new phenomena (see below) we report here. Charge-ordered phases including stripes,^{60,61,62} disorder pinned electronic liquid crystal,⁶³ strong-coupling spin- and charge-density waves,⁶⁴ and, recently, hole-pair crystals⁶⁵ have been proposed to exist in underdoped cuprates. Each of these phenomena would yield both *LDOS*- and topographic-modulations. But again, it remains theoretically unexplored whether these theories

can account for our observations that in the ZTPG regions (i) a characteristic new tunneling spectrum exists, (ii) the \vec{q}^* modulations appear only above a relative high energy (≈ 65 meV), (iii) they exhibit an incommensurate wavevector $\vec{q} = (\pm 2\pi/4.5a_0, 0)$ and $(0, \pm 2\pi/4.5a_0) \pm 15\%$, (iv) they exhibit the same spatial phase for positive and negative biases - so that the filled-state density maxima coincide with the empty-state-density maxima, and (iv) the \vec{q}^* modulations are replaced by the dispersive quasi-particle interference signals at sub-gap energies. A further point is that the predicted strong breaking of the 90° rotation symmetry in the stripe scenario is not observed in any of the STM studies, but again, it may be possible that this is due to the presence of strong disorder. For all these reasons the precise identity of the charge-order state in strongly underdoping Bi-2212 remains elusive.

The data reported here also motivate a new conjecture on the evolution of electronic structure with reduced doping in Bi-2212. In \vec{r} -space, we identify two extreme types of *LDOS* spectra (Fig. 6B). The first exhibits clear coherence peaks at the gap edge and dominates near-optimal samples. The second type (ZTPG-spectrum) exhibits a V-shaped gap over a much wider energy range and dominates in strongly underdoped samples. We associate the former with a pure d-wave superconducting state and conjecture that the latter reflects a zero temperature charge ordered state existing at sufficiently low dopings in the pseudogap regime. If the whole Bi-2212 sample were homogeneous and consisted of only one of the above phases, then, in \vec{k} -space, quasi-particle peaks would exist all along the Fermi surface in the pure d-SC phase, but only on a finite arc around the gap nodes in the charge ordered phase with the zone face states being incoherent due to localization. This may indeed be the case in $\text{Na}_x\text{Ca}_{2-x}\text{CuO}_2\text{Cl}_2$.^{27,46} In Bi-2212 the reality is more complicated. In optimally doped samples, more than 98% of the surface area exhibit dSC spectra (Fig. 3A,B). As doping falls the ZTPG regions appear and grow in significance until as doping approaches $p \approx 0.1$, almost 60% of the area exhibits the ZTPG characteristics and the associated charge-order (Fig. 3E). From this trend, it is reasonable to expect that, at even lower doping in the zero temperature pseudogap phase, 100% of the sample would exhibit the ZTPG characteristics and be charge-ordered.

In a spatially disordered situation, the probability of occurrence of the two types of phenomena evolves continuously with doping in a fashion related to the evolution of the gapmaps in Fig. 3. Therefore, properties which average over nanoscale phenomena would appear to evolve smoothly between the two extremes. Experimental results which are relevant to this proposal include, for example, the doping dependence of the ARPES ($\pi, 0$) peak,^{2,19,20,24} the specific heat jump at the superconducting phase transition,² and the c-axis conductivity.² Due to the heterogeneous mixture of the dSC and the ZTPG regions, it is difficult for a spatially averaged experiment like ARPES to discern the properties of the ZTPG re-

gion. However, the well-known tendency of the coherent quasiparticle peaks near the zone face to be suppressed by underdoping,^{19,20,24} is consistent with our conjecture. The specific heat jump at the superconducting transition is a characteristic specifically of a dSC phase and not of the charge-ordered ZTPG phase. Hence, the declining specific heat jump as a function of underdoping^{2,66} is also consistent with our hypothesis. Finally, due to tunneling matrix element effects, c-axis tunneling senses the zone-face quasiparticles instead of the nodal ones. Hence the decrease of the c-axis conductivity with underdoping² also seems consistent with our suggestion. Further inter-comparison between the results of these experimental techniques will be required to explore these proposals.

One may also wonder if the charge-ordered ZTPG phase could actually be the source of the high temperature pseudogap phenomena.² Since the charge-order would melt as a function increasing temperature, the answer to this question it is not clear. If the charge order melting temperature were actually the pseudogap temperature T^* , then of course, the entire pseudogap phenomena would be caused by the ZTPG phase. On the other hand if the charge melting temperature were lower than the pseudogap temperature T^* , then there would exist yet another mechanism that gaps the spin excitations at the pseudogap crossover.

Independent of these conjectures on doping-dependence of spatially-averaged observables, the data reported here represent two significant advances. First, a charge ordered state competing with superconductivity exists in strongly underdoped Bi-2212 and second, the charge-ordered regions and the d-SC regions share the same low energy nodal quasiparticles. New microscopic theories for the electronic structure of underdoped cuprates are therefore required to explain, not only the unusual characteristics of the charge order phenomenon and how it competes with superconductivity for spectral density at the zone-face, but also how it meshes so smoothly with the nodal superconductivity at low energies.

Figure 1

A schematic phase diagram of the cuprates. Note that the region of our studies is between $0.1 < p < 0.2$ and near the zero temperature axis of this diagram where the magnetically disordered spin glass region coexists with the superconductivity.

Figure 2

A The gapmap $\Delta(\vec{r})$ calculated from a $g(\vec{r}, E)$ data set which was measured in a 55 nm field of view (FOV) with 256^2 pixels; inset topography in this FOV. **B** The unprocessed linecut $g(\vec{r}, E)$ connection a region with sharp coherence peaks with a region designated ZTPG (see text), along the red line in Fig. 2A. **C** The measured $g(\vec{r}, E = -12\text{meV})$ in the identical FOV as 2A. **D** calculated from **C** (the reciprocal space location of the Bi or Cu atoms are labeled $(2\pi, 0)$). These five types of measurements are used in concert to study the doping dependence of electronic structure in Bi-2212.

Figure 3

A-E Measured $\Delta(\vec{r})$ for five different hole-doping levels. **F**. The average spectrum associated with each gap value in a given FOV. They were extracted from the $g(\vec{r}, E)$ that yielded Fig. 3C but the equivalent analysis for $g(\vec{r}, E)$ at all dopings yields results which are indistinguishable. The coherence peaks can be detected in #'s 1-4.

Figure 4

A-C Examples of measured $g(\vec{q}, E)$ for a variety of energies E as shown at three doping levels.

Figure 5

A. A schematic representation of the 1st Brillouin zone and Fermi surface location of Bi-2212. The flat-band regions near the zone face are shaded in blue. The eight locations which determine the scattering within the octet model are show as red circles and the scattering vectors which connect these locations are show as arrows labeled by the designation of each scattering vector. **B**. Measured dispersions of the LDOS-modulations \vec{q}_1 , \vec{q}_5 and \vec{q}_7 for the 3 dopings whose unprocessed data is shown in Fig.4. We chooses this set of three \vec{q} -vectors because they exhibit the maximum intensity of any set sufficient to independently determine the locus of scattering $\vec{k}_s(E)$ for all dopings. **C**. Calculated loci of scattering $\vec{k}_s(E)$ for all 3 dopings. The blue line is a fit to the 89KOD data.

Figure 6

A A high-resolution 46nm square gapmap from a strongly underdoped sample. **B**. Examples of representative spectra from (1) nanoscale regions exhibiting coherence peaked spectra with $\vec{q} = \vec{Q}$ LDOS-modulations at $E = \Delta(\vec{r})$ (red) and (2) from regions exhibiting ZTPG spectra (black). The locations where these spectra occur are shows as small dots in **A**. **C**. The mask identifying regions with $\Delta < 65$ meV from the ZTPG regions calculated from gapmap in **A**. **D**. Dispersion of $\vec{q}_1(E)$ in regions with coherence peaked spectra $\Delta < 65$ meV is shown in red. There are no modulations at any higher energies within our range. Dispersion of $\vec{q}_1(E)$ in regions with ZTPG spectra for $E < 36$ meV (black symbols). The red squares in Fig.5B represent a combination of these two (indistinguishable) dispersions in this range. For $E > 65$ meV, the wavevector of the new modulations in ZTPG regions are shown in black. To within our uncertainty they do not disperse and exhibit $\vec{q}^* = (\pm 2\pi/4.5a_0, 0)$ and $(0, \pm 2\pi/4.5a_0) \pm 15\%$.

Figure 7

AThe image of $g(\vec{r}, E)$ masked by Fig.6C and then summed from 65 meV to 150 meV : $\Gamma_{65}^{150}(\vec{r}) = \Sigma_{65}^{150} g(\vec{r}, E)|_{\delta > 65}$. The light grey regions are outside the mask. This FOV is 46nm square and a careful examination reveals a 'checkerboard' modulation occurring within the regions inside the mask. The equivalent image for $\Gamma_{65}^{150}(\vec{r}) = \Sigma_{65}^{150} g(\vec{r}, E)|_{\delta < 65}$ is featureless except for Bi atom locations, and the supermodulation which is at 45° to the modulation in **A**. **B**. Fourier transform **A**. The Bi atom locations are circled in orange. A square of diffuse maxima are observed surrounding the central

point. The inset shows the plot of the Fourier transform amplitude along the line shown. It reveals a maximum at $\vec{q}^* = (\pm 2\pi/4.5a_0, 0)$ and $(0, \pm 2\pi/4.5a_0) \pm 15\%$ as indicated by the arrow. **C.** The magnitude of the Fourier transform of the masked topographic image, taken at 150 mV and 150 pA, along the $\vec{q}_{topo} || (2\pi, 0)$ direction is modulated with $\vec{q}_{topo} = (\pm 2\pi/5a_0, 0)$ and $(0, \pm 2\pi/5a_0) \pm 25\%$ (black squares the black line is a guide to the eye). Fourier transforms of the complementary part of the topography (from < 65 meV regions not exhibiting ZBTG spectra) shows no such modulations at any wavelengths near this \vec{q}_{topo} (red triangles the red line is a guide to the eye). The difference between these two Fourier transform intensities is shown in blue and shows the degree to which the ZTPG region shows topographic modulations undetectable elsewhere. The relative weakness of the topographic modulations at \vec{q}_{topo} is because of the logarithmic

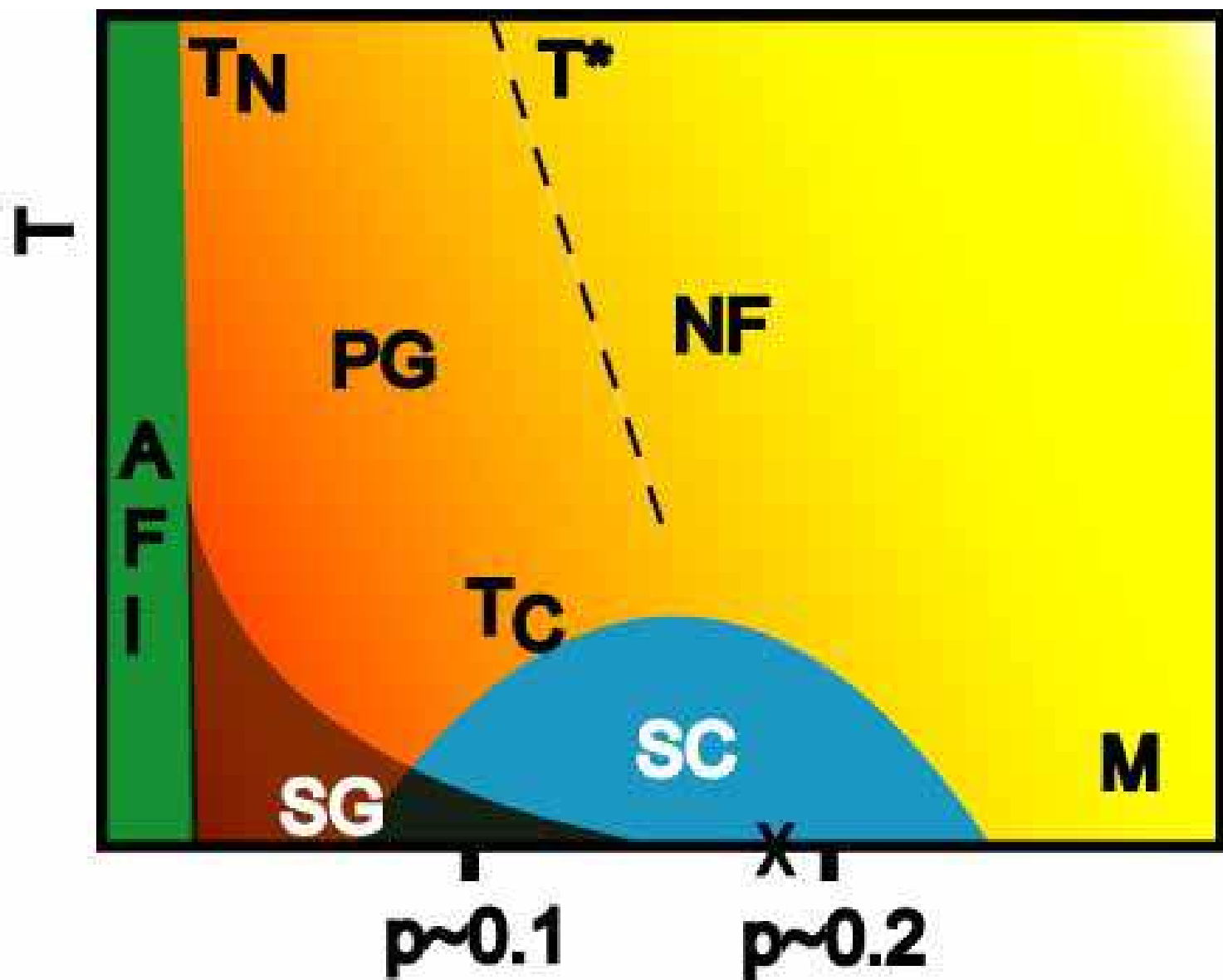
sensitivity of constant-current topography to net charge modulation. **D.** A plot of the amplitude of the \vec{q}_1 LDOS modulation as a function of $|\vec{q}_1|$ for the sample data as in Fig.3C, 4E, 5D. The maximum intensity of the modulations in the ZTPG regions occurs at $|\vec{q}_1| = 2\pi/4.8a_0 10\%$. No special scattering is observed of the quasiparticles in the dSC regions.

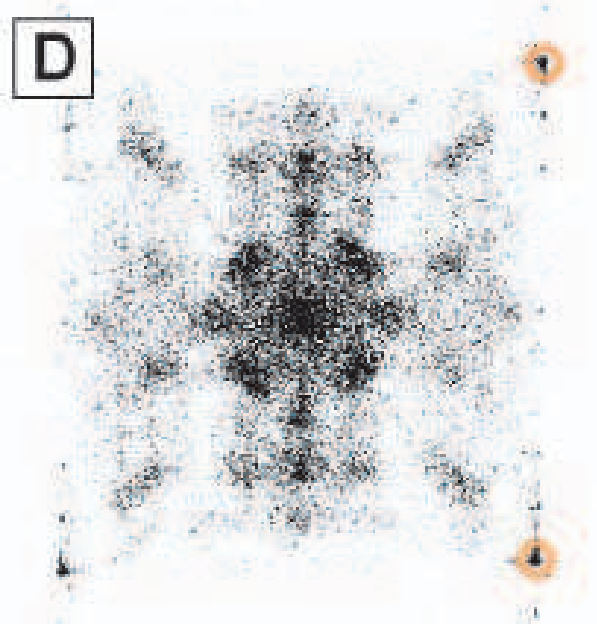
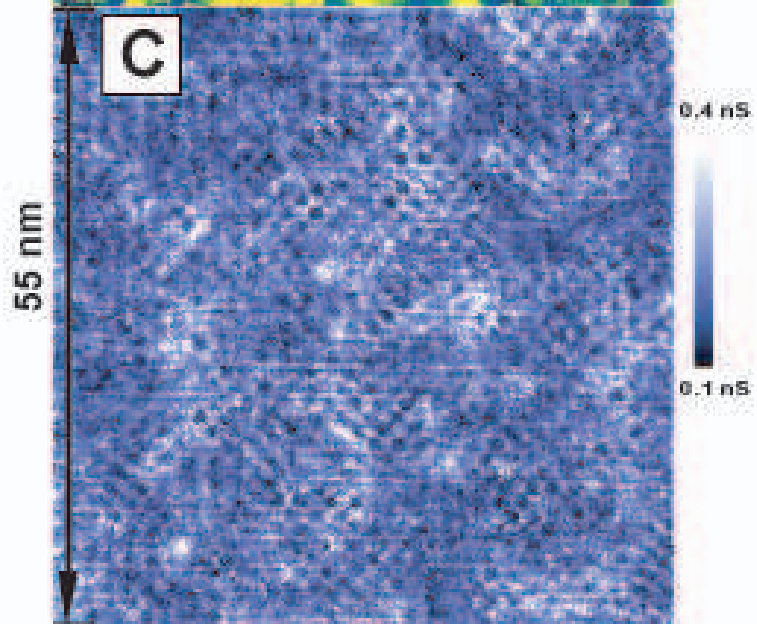
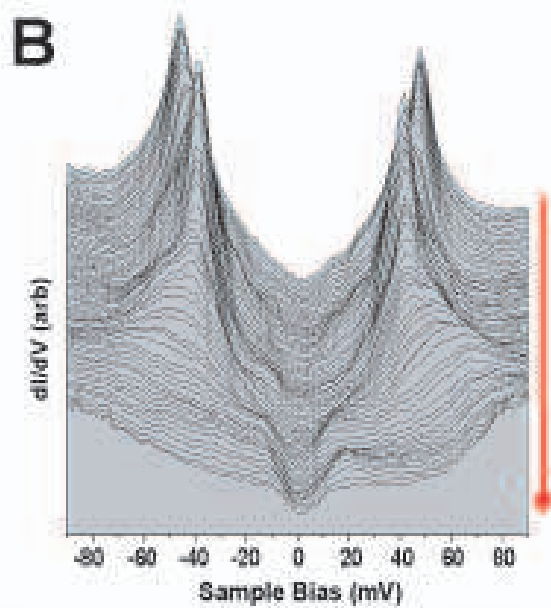
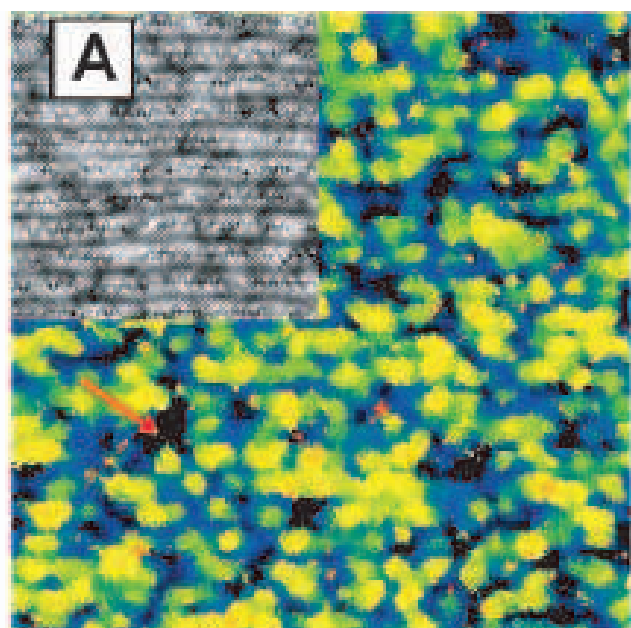
Acknowledgments

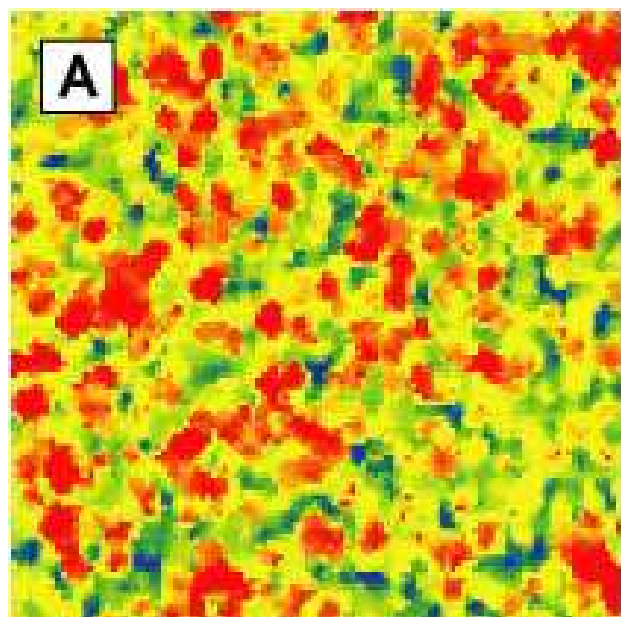
We acknowledge and thank A. V. Balatsky, S. Chakravarty, M. P. A. Fisher, T. Hanaguri, S. Kivelson, P. A. Lee, A. Millis, D. Pines, S. Sachdev, J. Sethna, T. Uemura, A. Yazdani, J. Zaanen, and S.-C. Zhang for very helpful discussions and communications.

-
- ¹ J. Orenstein and A. J. Millis, *Science* **288**, 468 (2000).
 - ² T. Timusk and B. Statt, *Rep. Mod. Phys.* **62**, 61 (2000).
 - ³ M. Norman and C. Pepin, *cond-mat/0302347*.
 - ⁴ K. Yamada, C. H. Lee, K. Kurahashi, J. Wada, S. Wakimoto, S. Ueki, H. Kimura, Y. Endo, S. Hosoya, G. Shirane, et al., *Phys. Rev. B* **67**, 6165 (1998).
 - ⁵ C. Niedermayer, C. Bernhard, T. Blasius, A. Golnik, A. Moodenbaugh, and J. Budnick, *Phys. Rev. Lett.* **80**, 3843 (1998).
 - ⁶ C. M. Varma, Z. Nussinov, and W. van Saarloos, *Phys. Rep.* **361**, 267 (2002).
 - ⁷ Y. Uemura, *Solid State Commun.* **126**, 23 (2002).
 - ⁸ C. Panagopoulos, J. L. Tallon, B. D. Rainford, J. R. Cooper, C. A. Scott, and T. Xiang, *Solid State Commun.* **126**, 47 (2002).
 - ⁹ T. Cren, D. Roditchev, W. Sacks, and J. Klein, *Europhys. Lett.* **54**, 84 (2001).
 - ¹⁰ S. H. Pan, J. P. O'Neil, R. L. Badzey, C. Chamon, H. Ding, J. R. Engelbrecht, Z. Wang, H. Eisaki, S. Uchida, A. K. Gupta, et al., *Nature* **413**, 282 (2001).
 - ¹¹ C. Howald, P. Fournier, and A. Kapitulnik, *Phys. Rev. B* **64**, 100504 (2001).
 - ¹² K. M. Lang, V. Madhavan, J. E. Hoffman, E. W. Hudson, and J. C. D. H. Eisaki, S. Uchida, *Nature* **415**, 412 (2002).
 - ¹³ A. Matsuda, T. Fujii, and T. Wantanabe, *Physica C* **388-389**, 207 (2003).
 - ¹⁴ Y. Hoshaka, T. Hanaguri, K. Kitazawa, M. Azuma, M. Takano, and H. Tagaki, *J. Low Temp. Phys.* **131**, 299 (2003).
 - ¹⁵ J. Hasse, C. P. Slichter, and C. T. Milling, *J. Supercond.* **15**, 339 (2002).
 - ¹⁶ P. M. Singer, A. W. Hunt, and T. Imai, *Phys. Rev. Lett.* **88**, 047602 (2002).
 - ¹⁷ J. Loram, J. Tallon, and W. Liang, *Phys. Rev. B* **69**, 060502 (2004).
 - ¹⁸ T. Schneider, *cond-mat/0308595*.
 - ¹⁹ A. Damascelli, Z. Hussain, and Z.-X. Shen, *Rev. Mod. Phys.* **75**, 473 (2003).
 - ²⁰ J. C. Campuzano, M. R. Norman, and M. Randeria, *cond-mat/0209476*.
 - ²¹ P. D. Johnson, A. Fedorov, and T. Valla, *J. Electron Spectroscopy* **117**, 153 (2001).
 - ²² A. V. Fedorov, T. Valla, P. D. Johnson, Q. Li, G. D. Gu, and N. Koshizuka, *Phys. Rev. Lett.* **82**, 2179 (1999).
 - ²³ A. G. Loeser, Z.-X. Shen, M. C. Schabel, C. Kim, M. Zhang, A. Kapitulnik, and P. Fournier, *Phys. Rev. B* **56**, 14185 (1997).
 - ²⁴ D. L. Feng, D. H. Lu, K. M. Shen, C. Kim, H. Eisaki, A. Damascelli, R. Yoshizaki, J. i. Shimoyama, K. Kishio, G. D. Gu, et al., *Science* **289**, 277 (2000).
 - ²⁵ M. R. Norman, H. Ding, M. Randeria, J. C. Campuzano, T. Yokoya, T. Takeuchi, T. Takahashi, P. G. T. Mochiku, K. Kadowaki, and D. G. Hinks, *Nature* **392**, 157 (1998).
 - ²⁶ T. Yoshida, X. J. Zhou, T. Sasagawa, W. L. Yang, P. V. Bogdanov, A. Lanzara, Z. Hussain, T. Mizokawa, A. Fujimura, H. Eisaki, et al., *Phys. Rev. Lett.* **91**, 027001 (2003).
 - ²⁷ F. Ronning, T. Sasagawa, K. Koshaka, K. M. Shen, A. Damascelli, C. Kim, T. Yoshida, N. P. Armitage, D. H. Liu, D. L. Feng, et al., *Phys. Rev. B* **67**, 165101 (2003).
 - ²⁸ N. Gedik, J. Orenstein, R. Liang, D. A. Bonn, and W. N. Hardy, *Science* **30**, 1410 (2003).
 - ²⁹ J. E. Hoffman, E. W. Hudson, K. M. Lang, V. Madhavan, H. Eisaki, S. Uchida, and J. C. Davis, *Science* **295**, 466 (2002).
 - ³⁰ J. E. Hoffman, K. McElroy, D.-H. Lee, K. M. Lang, H. Eisaki, S. Uchida, and J. C. Davis, *Science* **297**, 1148 (2002).
 - ³¹ K. McElroy, R. W. Simmonds, J. E. Hoffman, D.-H. Lee, J. Orenstein, H. Eisaki, S. Uchida, and J. C. Davis, *Nature* **422**, 520 (2003).
 - ³² M. Vershinin, S. Misra, S. Ono, Y. Abe, Y. Ando, and A. Yazdani, *Science* **303**, 1995 (2004).
 - ³³ N. Miyakawa, P. Guptasarma, J. F. Zasadzinski, D. G. Hinks, and K. E. Gray, *Phys. Rev. Lett.* **80**, 157 (1998).
 - ³⁴ J.-X. Zhu, I. Martin, and A. R. Bishop, *Phys. Rev. Lett.* **89**, 067003 (2002).
 - ³⁵ J. M. Byers, M. E. Flatté, and D. J. Scalapino, *Phys. Rev. Lett.* **67**, 100506 (1993).
 - ³⁶ D. Zhang and C. S. Ting, *Phys. Rev. B* **67**, 100506 (2003).
 - ³⁷ Q. Wang and D.-H. Lee, *Phys. Rev. B* **67**, 020511 (2003).
 - ³⁸ J.-X. Zhu, W. Kim, C. S. Ting, and J. P. Carbotte, *Phys.*

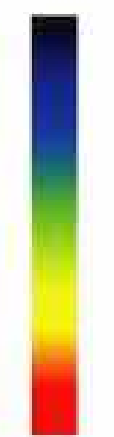
- Rev. Lett. **87**, 197001 (2001).
- ³⁹ L. Capriotti, D. J. Scalapino, and R. D. Sedgewick, cond-mat/0302563.
- ⁴⁰ L. Zhu, W. A. Atkinson, and P. J. Hirschfeld, Phys. Rev. B **69**, 060503 (2004).
- ⁴¹ C.-T. Chen and N.-C. Yeh, cond-mat/0307660.
- ⁴² T. Pereg-Barnea and M. Franz, Phys. Rev. B **68**, 180506(R) (2003).
- ⁴³ C. Bena, S. Chakravarty, J. Hu, and C. Nayak, cond-mat/0311299.
- ⁴⁴ C. Renner, B. Revaz, K. Kodowaki, I. Marggion-Aprile, , and O. Fischer, Phys. Rev. Lett. **80**, 3606 (1998).
- ⁴⁵ S. H. Pan, E. W. Hudson, A. K. Gupta, K.-W. Ng, H. Eisaki, S. Uchida, and J. C. Davis, Phys. Rev. Lett. **85**, 1536 (2000).
- ⁴⁶ T. Hanaguri, C. Lupien, Y. Kohsaka, D.-H. Lee, M. Azuma, M. Takano, H. Takagi, and J. C. Davis, to be published.
- ⁴⁷ T. Senthil and M. P. A. Fisher, Phys. Rev. B **62**, 7850 (1993).
- ⁴⁸ M. Vojta, Y. Zhang, and S. Sachdev, Phys. Rev. B **62**, 6721 (2000).
- ⁴⁹ N. Jogelkar, A. H. C. Neto, and A. V. Balatsky, cond-mat/0304536.
- ⁵⁰ O. Parcollet, G. Biroli, and G. Kotliar, cond-mat/0308577.
- ⁵¹ D. Podolsky, E. Demler, K. Damle, and B. I. Halperin, Phys. Rev. B **67**, 094514 (2003).
- ⁵² D.-H. L. Henry C. Fu, J. C. Davis, cond-mat/0403001.
- ⁵³ J. Tranquada, B. Sternlieb, J. Axe, Y. Nakamura, and S. Uchida, Nature **375**, 6532 (1995).
- ⁵⁴ C. Howald, H. Eisaki, N. Kaneko, M. Greven, and A. Kapitulnik, Phys. Rev. B **67**, 014533 (2003).
- ⁵⁵ I. Affleck and J. B. Marston, Phys. Rev. B **37**, 3774 (1988).
- ⁵⁶ P. A. Lee, cond-mat/0307508.
- ⁵⁷ S. Chakravarty, R. B. Laughlin, D. K. Morr, and C. Nayak, Phys. Rev. B. **63**, 094503 (2001).
- ⁵⁸ C. M. Varma, Phys. Rev. B. **55**, 14554 (1997).
- ⁵⁹ J. i. Kishine, P. A. Lee, and X.-G. Wen, Phys. Rev. Lett. **86**, 5365 (2001).
- ⁶⁰ J. Zaanen and O. Gunnarsson, Phys. Rev. B **40**, 7391 (1989).
- ⁶¹ S. A. Kivelson, E. Fradkin, and V. J. Emery, nature **393**, 550 (1998).
- ⁶² U. Lw, V. J. Emery, K. Fabricius, and S. A. Kivelson, Phys. Rev. Lett. **72**, 1918 (1994).
- ⁶³ S. A. Kivelson, I. P. Bindloss, E. Fradkin, V. Oganesyan, J. M. Tranquada, A. Kapitulnik, and C. Howald, Rev. Mod. Phys. **75**, 1201 (2003).
- ⁶⁴ S. Sachdev, Rev. Mod. Phys. **75**, 913 (2003).
- ⁶⁵ H.-D. Chen, S. Capponi, F. Alet, and S.-C. Zhang, cond-mat/0312660.
- ⁶⁶ J. W. Loram, J. Luo, J. R. Cooper, W. Y. Liang, and J. L. Tallon, Phys. Rev. B **62**, 59 (2001).



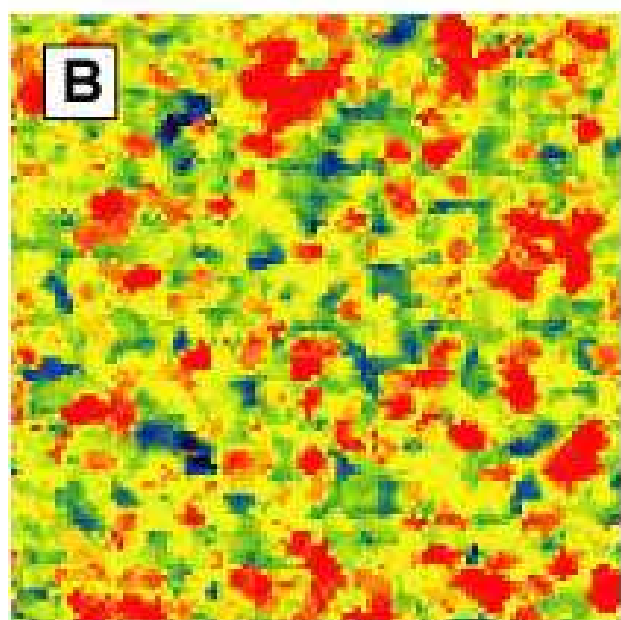
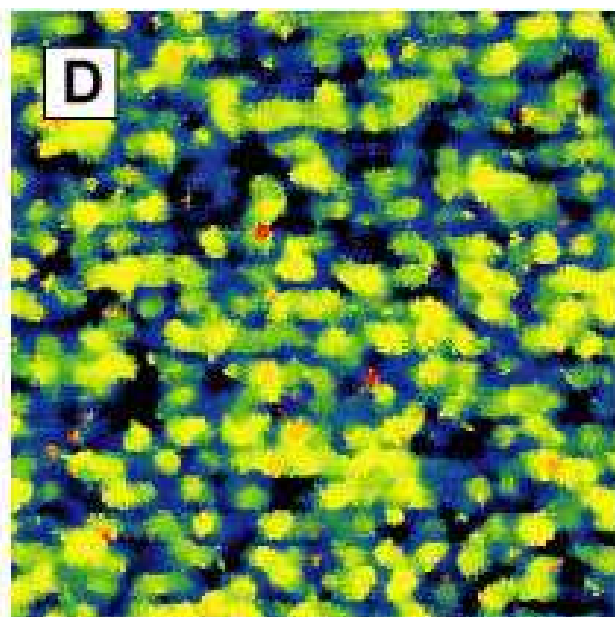




70 mV



20 mV



50 nm

